OPEN ACCESS

Spanish Journal of Agricultural Research 22 (4)
October-December, 2024, 20452
ISSN-L: 1695-971X, eISSN: 2171-9292
https://doi.org/10.5424/sjar/2024224-20452

RESEARCH ARTICLE

Detection of mite infested saffron plants using aerial imaging and machine learning classifier

Hossein Sahabi[1,2*] and Jalal Baradaran-Motie[3*]

[1]Department of Plant Production, University of Torbat Heydarieh, Torbat Heydarieh, 9516168595 Iran. [2]Saffron Institute, University of Torbat Heydarieh, Torbat Heydarieh, 9516168595 Iran. [3]Department of Biosystems Engineering, Ferdowsi University of Mashhad, Mashhad, 9177948974 Iran.

***Correspondence** should be addressed to Hossein Sahabi:h.sahabi@torbath.ac.ir or
Jalal Baradaran-Motie: j.baradaran@um.ac.ir

Abstract

Aim of study: To evaluate and develop a machine learning code that uses aerial images in visible and near infrared (NIR) spectra to detect mite-infested Saffron (*Crocus sativus* L.) plants through processing the spectral indices to classify healthy and diseased plants. This leads to the identification of the concentration points of the bulb mites and the estimation of the percentage of infestation in the field.

Area of study: Khorasan-Razavi province, Torbat-Heydarieh, Iran.

Material and methods: Five fields were randomly selected and their red-green-blue (RGB), as a typical visible spectral image, and NIR images were taken in two consecutive years. Seven spectral vegetation indices for NIR images including NIR-band, Red-band, normalized difference vegetation index (NDVI), ratio vegetation index (RVI), difference vegetation index (DVI), difference red-nir ratio (DRN) and infrared percentage vegetation index (IPVI); and twelve indices for RGB images inlcuding red-band, green-band, blue-band, visible-band difference vegetation index (VDVI), visible atmospheric resistant index (VARI), triangular greenness index (TGI), normalized difference greenness index (NDGI), normalized green blue difference index (NGBDI), modified green red vegetation index (MGRVI), red green blue vegetation index (RGBVI), vegetative index (VEG) and excess of green index (EXG), were extracted and analysed. In order to detect affected plants, two support vector machine (SVM) classifiers with radial basis function (RBF) kernels were used separately for NIR and RGB images.

Main results: The average accuracy of the SVM classifier models were estimated to be 82.3% for NIR images and 91.4% for RGB images during the test phase. Also, the accuracy of the developed models when evaluated in the field with respect to the confusion matrix method was 75.6% and 80.3% for the classification models for NIR and RGB images, respectively.

Research highlights: RGB images were able to distinguish infested plants with better accuracy. Processing aerial images of lightweight drones could speed up the inspection of vast saffron fields.

keywords: Aerial imaging; Classification; Image processing; *Crocus sativus*; Support vector machine.

Detección de plantas de azafrán infestadas por ácaros mediante imágenes aéreas y un clasificador de aprendizaje automático

Resumen

Objetivo del estudio: Evaluar y desarrollar un código de aprendizaje automático que utilice imágenes aéreas en los espectros visible e infrarrojo cercano (NIR) para detectar plantas de azafrán (*Crocus sativus* L.) infestadas por ácaros mediante el procesamiento de índices espectrales para clasificar plantas sanas y enfermas. Esto permite identificar los puntos de concentración de los ácaros del bulbo y estimar el porcentaje de infestación en el campo.

Área de estudio: Provincia de Jorasán-Razaví, Torbat-Heydarieh, Irán.

Materiales y métodos: Cinco campos fueron seleccionados al azar, y se tomaron sus imágenes en rojo-verde-azul (RGB), como una imagen espectral visible típica, e imágenes en infrarrojo cercano (NIR) en dos años consecutivos. Se extrajeron y analizaron siete índices de vegetación espectrales para las imágenes NIR, que incluyeron *NIR-band, red-band, normalized difference vegetation index (NDVI), ratio vegetation index (RVI), difference vegetation index (DVI), difference Red-NIR ratio (DRN) and infrared percentage vegetation index (IPVI)*; y doce índices para las imágenes visibles RGB, que incluyeron *red-band, green-band, blue-band, visible-band difference vegetation index (VDVI), visible atmospheric resistant index (VARI), triangular greenness index (TGI), normalized difference greenness index (NDGI), normalized green blue difference index (NGBDI), modified green red vegetation index (MGRVI), red green blue vegetation index (RGBVI), vegetative index (VEG) and excess of green index (EXG)*. Para detectar las plantas afectadas, se utilizaron dos clasificadores de Máquinas de Soporte Vectorial (SVM) con núcleos de Función de Base Radial (RBF) de forma separada para las imágenes NIR y RGB.

Resultados principales: La precisión promedio de los modelos clasificadores SVM se estimó en un 82.3% para las imágenes NIR y un 91.4% para las imágenes visibles durante la fase de prueba. Además, la precisión de los modelos desarrollados al ser evaluados en campo con respecto al método de matriz de confusión fue del 75.6% y 80.3% para los modelos de clasificación de imágenes NIR y RGB, respectivamente.

Aspectos destacados de la investigación: Las imágenes RGB lograron distinguir plantas infestadas con mejor precisión. El procesamiento de imágenes aéreas de drones de bajo peso podría acelerar la inspección de grandes campos de azafrán.

Palabras clave: Imágenes aéreas; Clasificación; Procesamiento de imágenes; *Crocus sativus*; Máquina de soporte vectorial.

The translation of the title, abstract, and keywords from the original version in English to Spanish has been generated using OpenAI, ChatGPT GPT-4o mini (2024).

La traducción al español del título, resumen y palabras clave de la versión original en inglés ha sido generada utilizando OpenAI., ChatGPT GPT-4o mini (2024).

Citation: Sahabi, H; Baradaran-Motie, J (2024). Detection of mite infested saffron plants using aerial imaging and machine learning classifier. Spanish Journal of Agricultural Research, Volume 22, Issue 4, 20452. https://doi.org/10.5424/sjar/2024224-20452

Received: 11/05/2023. **Accepted**: 27/06/2024. **Published**: 27/11/24

Introduction

Saffron, *Crocus sativus* L., a valuable member of the Liliaceae family, possesses one of the most expensive stigmas in the world, prized for its industrial and medicinal applications (Caiola & Canini, 2010; Golmohammadi, 2014). This perennial herb, typically reaching 10-30 cm in height, features a hard, round corm covered in thin, brown scales. It produces 5-11 leaves, often emerging simultaneously or shortly after flowering (Cardone et al., 2020). The dried red stigma of saffron is the coveted final product. It occupies a prominent position in the agricultural economies of Iran, Spain, Greece, Afghanistan, and certain Middle Eastern countries(Mzabri et al., 2019). Given the widespread use of saffron, enhancing its production, yield, and quality is a critical objective (Kafi et al., 2006).

One significant challenge hindering saffron's quantitative and qualitative yield is the damage inflicted by pests and diseases. Saffron virus diseases, saffron corm rot, saffron dry rot (*Burkholderia gladioli*), and the saffron bulb mite (*Rhizoglyphus robini*) are among the primary biotic factors affecting stigma quality (Zakiaghl et al., 2021). The saffron bulb mite poses a particular threat to saffron corms (Kafi et al., 2006). This pest inflicts both direct and indirect damage. Directly, it tears into the corm's healthy tissue with its claws and feeds on its contents. Indirectly, it creates entry points for parasitic and saprophytic fungi, leading to rotting, blackening, and ultimately, the destruction of infected tissue (Rahimi et al., 2018).

Identifying saffron pathogens involves various laboratory and field methods (Kafi et al., 2006; Zakiaghl et al., 2021). The saffron bulb mite often infests corms from the wounds and sometimes from healthy parts, and as it feeds and tunnels inside the corms, it begins to multiply and form cavities in the corms (Tavakkoli-Korghond & Sahebzadeh, 2022). Infested plants exhibit thinner, shorter leaves that fall prematurely. A common symptom of both mite and fungal damage is reduced photosynthesis (Genc et al., 2008) and discolored leaves, often turning light green or yellow. While these leaf changes are not noticeable, they may not be readily distinguishable to the human eye, making it difficult to identify infested plants from healthy ones. Traditional detection of mite damage in saffron bulbs requires farmers to inspect fields and physically remove bulbs from the soil. Aerial imaging offers a potential solution to expedite and enhance the accuracy of this process.

Early detection of infested plants is problematic, as visual symptoms often remain imperceptible until the infestation has spread significantly, resulting in substantial plant damage. Prompt recognition of mite infestation is crucial due to the disease's rapid propagation (Rahimi et al., 2018). Identifying areas affected by fungi resulting from saffron mite infestation can facilitate the strategic application of chemical control. This targeted approach, focusing solely on infested regions, minimizes pesticide or fungicide consumption compared to treating the entire field. Precision farming technologies offer a promising solution by enabling early detection of pests and diseases, leading to targeted variable-rate spraying (Zakiaghl et al., 2021; Baradaran Motie et al., 2023).

Various studies have explored the use of image processing techniques to identify plant infestation by pests or diseases using hyperspectral, multispectral, Red-Green-Blue (RGB) cameras, with demonstrated effectiveness (Abdulridha et al., 2020; Li et al., 2021). Research has established a significant difference in spectral absorbance between healthy and infested plants within the 750-900 nm spectral range (Basati et al., 2018). Image capture can be performed from ground-based systems or aerial platforms. Subsequently, these images are processed using computer software employing machine learning and other techniques (Li et al., 2021). Ground imagery offers greater precision due to the controllability of factors affecting image quality (e.g., light, reflection). While aerial imaging is influenced by certain uncontrolled factors, it is favored by researchers owing to its rapid acquisition speed and ability to monitor extensive areas (Sankaran et al.,

Table 1. Some applications of image processing for the detection of plant diseases.

Target plant	Application	spectral range (nm)	Wavelength/ index selection method [1]	Indices used [2]	Accuracy (%)	Method of modelling [3]	Source
Rice	Detection of brown spots on leaves	350-2400	DA	NDVI, SAVI, green NDVI	86	MLR	(Yang et al., 2007)
Sugar beet	Diagnosis of some diseases in sugar beet leaves	400-1050	DT	NDVI, SI, SIPI, PSSRa, ARI, REP, mCAI	65-90	SVM	(Rumpf et al., 2010)
Cotton	Feasibility of disease diagnosis	RGB	GA	Basic RGB and YCbCr channels	90.5	SVM	(Gulhane & Gurjar, 2011)
Whiteflies	Detection of pests in the greenhouse based on leaf symptoms	RGB	Shape and colour properties	Basic RGB channels	90	SVM	(Rupesh & Mundada, 2013)
Wheat	Determining damage levels in wheat kernels caused by Sunn pest	950-1650	N/A	Full spectrum	88.2	PLS-DA	(Armstrong et al., 2019)
Squash	Detecting powdery mildew disease in squash using hyperspectral imaging	388-1012	Based on Vis	NDVI, greenNDVI, mCAI, ARI, SIPI, PRI	89	RBF-ANN	(Abdulridha et al., 2020)
Tomato	Tomato disease detection from leaves image	RGB	C-GAN	C-GAN layers	97	DenseNet121	(Abbas et al., 2021)
Potato	Early detection of *Alternaria solani* in potatoes	350-2500	N/A	Full spectrum	75	PLS-DA	(Abdelghafour et al., 2023)

[1] DA: stepwise Discriminant Analysis. DT: Decision Tree. GA: genetic algorithm. C-GAN: Conditional Generative Adversarial Network. N/A: Not Available.[2] NDVI: Normalized diffrence vegetation index. SAVI: Soil Adjusted Vegetation Index. SI: Simple Ratio (R_{800}/R_{650}). SIPI: Structure Insensitive Vegetation Index. PSSRa: Pigments Specific Simple Ratio. ARI: Anthocyanin Reflectance Index. REP: Red Edge Position. mCAI: modified chlorophyll absorption integral. RGB: red, green, blue bands. VI: vegetation index. [3] MLR: Multiple Linear Regression. SVM: Support Vector Machine. PLS-DA: Partial Least Squares Discriminant Analysis. RBF: Radial Basis Function. ANN: Artificial neural network.

2015). In many cases, results derived from aerial image processing are comparable in accuracy to those obtained from ground-based methods. Xiang & Tian (2011) reported a mere 1.5% difference between results obtained from drone-mounted multispectral cameras and ground-based surveys in evaluating herbicide application performance. While factors such as global positioning system (GPS) coordinate accuracy (Gomez et al., 2008), the number of ground control points, flight altitude, image resolution, and pixel spatial resolution influence the precision of aerial survey results, the choice of appropriate analysis software, including classification systems, artificial neural networks, and machine learning algorithms, can significantly impact accuracy. Abuleil et al. (2015), found that the k-nearest neighbors (kNN) algorithm outperformed artificial neural networks (ANN) and support vector machine (SVM) in detecting red clover (*Trifolium pratense*) ground cover using RGB images captured by unmanned aerial vehicles (UAV), achieving a 91% accuracy rate.

By extracting and processing spectral bands and calculating various indices such as the normalized difference vegetation index (NDVI), ratio vegetation index (RVI), and leaf area index (LAI), variations in plant health status within fields or gardens can be determined (Table 1). However, the optimal indicators may vary depending on the specific disease or pest. Examples include the correlation between grapevine leaf streak disease (GLSD) and the NDVI index in vineyards (di Gennaro et al., 2016) and the relationship between plant vegetation and the LAI (Ballesteros et al., 2014). To achieve the highest accuracy, simultaneous analysis of multiple plant indices is often necessary (Zarco-Tejada et al., 2013). For instance, Elarab et al. (2015) proposed the combined use of indices incorporating RGB, Near-Infrared (NIR), NDVI, LAI, green model, and thermal imaging data to assess chlorophyll levels in plants (Oat plant case study).

Despite extensive research on the application of multispectral imaging in detecting numerous plant diseases, literature on its use in identifying saffron bulb infection using machine learning techniques remains limited. Therefore, the primary objective of this study was to investigate the feasibility of employing spectral features from visible and near-infrared drone images to differentiate infested saffron plants from healthy ones using support vector machine (SVM) models. The SVM models, a powerful pattern recognition method for binary classification, has demonstrated its efficacy in various research contexts (Baradaran Motie et al., 2023). Additional objectives of this study included: i) Analyzing and comparing various vegetation indices. ii) Identifying the most effective indices for distinguishing infested plants. iii) Developing a MATLAB code for image analysis based on these indices to delineate contaminated areas in large fields and calculate the extent of infestation.

Material and methods

Experimental fields and plants

Field investigations were conducted during the phenological vegetation phase of saffron, spanning February to April, across five saffron fields in Torbat-Heydarieh (Khorasan-Razavi Province, northeast of Iran), situated at an average altitude of 1450 meters above sea level (Table 2). These fields employed furrow irrigation. The primary objective was to identify saffron plants damaged by mites. Prior to the investigation, manual inspections confirmed the presence of mite pests in the examined fields during the previous growing season.

Imaging devices - The cameras

This research employed a variety of imaging techniques. Initially, hyperspectral images of saffron leaves in both healthy and damaged states were captured within a laboratory setting. A desktop HYSPIM alpha visible-near infrared (Vis-NIR) hyperspectral camera (Hyspim, Sweden) was utilized for this purpose. Each pixel of the 2D image contained spectral data within the wavelength range of 400-950 nm at a resolution of 2 nm. The camera was positioned in a controlled dark room, and illumination was provided by four full-spectrum 50W halogen lamps (Osram, Germany). Subsequently, on-site imaging was conducted during ground and aerial surveys. A Survey2 NIR camera (MAPIR, USA), equipped with a Sony Exmor IMX206 16MP (Bayer RGB) sensor and an FOV of 82°

Table 2. Saffron fields selected for mite infestation monitoring and aerial imaging.

Site code	Field age[1] (year)	Soil type	Coordinates of the field centre
A1	3	Loam	N 59°20’55.0”E”4.0’35º18
A2	2	Loam	N 59°20’48.0”E”11.0’35º °18
A3	4	Sandy loam	N 59°20’40.0”E”60.0’ 35°17
A4	4	Loam	N 59°19’30.0”E”14.0’ 35°19
A5	4	Loam	N 59°22’44.0”E”13.0’ 35°18

[1] **Number of years after bulb cultivation**.

23mm f/2.8, was used to capture images in 850 nm (NIR) and 660 nm (visible region) bands. A Canon Powershot RGB camera, featuring a 1/2.55" CMOS sensor with 12MP effective pixels and a field of view (FOV) of 94° and f/2.2, was also employed.

A Phantom 3 SE (DJI, China) drone was utilized for aerial imaging. This drone is equipped with a 4K camera capable of recording video at 30 frames per second, a 1/2.3-inch CMOS sensor with 12 million effective pixels, a maximum flight time of 25 minutes, and a maximum transmission range of 5 kilometers. Its specially designed lens with an FOV of 94° is well-suited for aerial imaging. The NIR camera was subsequently mounted on a drone for aerial imaging.

Image acquisition and processing

To assess the feasibility of using spectral data to differentiate between healthy and infested saffron plants and to select the most appropriate spectral bands, twenty plants were sampled from each field. These plants were divided into two groups: healthy and infested. Hyperspectral imaging was conducted within the 400-900 nm spectral range. To identify the optimal bands for classification and validate camera performance, spectral signatures of healthy and infested saffron leaves were compared.

The field survey phase comprised two stages. During the first year, ground surveys were conducted to identify and harvest mite-infested saffron plants. Corms were separated from the surrounding soil and analyzed. Infested areas were marked with GPS coordinates for subsequent study of the infestation's effects on plants in the second year. Plants were divided into two groups: healthy and infected. Images were captured under consistent lighting conditions in both visible light and NIR spectra. Generally, the NIR images were preferred over RGB images due to their greater sensitivity to plant photosynthetic properties (Aslahishahri, et al., 2021). Image quality and resolution were evaluated at three flight altitudes: 5, 10, and 15m. Given the requirement for high-resolution images, a flight altitude of five meters was selected.

In the second stage, infested plants were labeled, and aerial images were acquired at the study site at a 5-meter altitude with 12-megapixel resolution. Images were captured using both RGB and NIR cameras in two consecutive years, March 2021 and 2022. At a height of 5 m, 12-megapixel images covered an approximate area of 7.7 × 6 m, resulting in a spatial resolution of 593 pixels/m² (6 pixels/cm).

The first-stage images of saffron plants (Figure 1) and the aerial images (Figure 2) were captured on sunny days between 10 a.m. and 12 p.m. During the first stage, 20 images were acquired, while the second stage involved capturing 20 aerial images from each of the five fields in both RGB and NIR bands. A total of 100 images (from the first stage) were used to train the classification algorithm. To create datasets of healthy and infested plants, plants were removed from the soil, and damage was confirmed. The first-stage images were employed to process and train the machine learning classification model, while the second set was used to evaluate the model's performance. Raw images underwent color analysis (extraction of color channels, histogram stretching, edge detection) before being processed. Image processing comprised four steps: pre-processing, segmentation, determination of vegetation indices, and image classification.

Figure 1. The images show mite-damaged saffron plants adjacent to healthy ones. Left: RGB image. Right: NIR (850 nm) image. This is an illustration of the first stage images from which the leaf reflection indices were extracted.

Figure 2. Second stage aerial image of field code A3 which infested by mite. Left: RGB image. Right: NIR image.

Software

Image processing was conducted using MATLAB software (version 2017). Two distinct codes were developed, one for analyzing RGB images and the other for NIR images. These codes followed a similar procedure, each consisting of five components:

1. Image acquisition.
2. Background removal and creation of a mask for leaves or utilization of a predefined mask.
3. Creation of a data matrix for all bands and calculation of vegetation indices.
4. Development of a dataset containing indices from both healthy and infested plants.
5. Creation and training of the SVM model.

Table 3. The examined indices in order to find the distinction between healthy and infested saffron plants.

Index group	Index[1]	Calculation method	Reference
NIR images	RED	*Reflectance in the red band*	(Xue & Su, 2017)
	NIR	*Reflectance in the near-infrared band*	(Mohamed et al., 2018)
	NDVI	$NDVI = \frac{NIR - RED}{NIR + RED}$	(Carreño-Conde et al., 2021)
	RVI	$RVI = \frac{RED}{NIR}$	(Xue & Su, 2017)
	DVI	$DVI = NIR - RED$	(Xue & Su, 2017)
	DRN	$DRN = \frac{RED - NIR}{RED}$	(Silleos et al., 2006)
	IPVI	$IPVI = \frac{NIR}{RED + NIR}$	(Crippen, 1990)
RGB images	*The reflectance of primary bands*	RED, GREEN, BLUE	(Abuleil et al., 2015)
	VDVI	$VDVI = \frac{2 \times Green - Red - Blue}{2 \times Green + Red + Blue}$	(Xue & Su, 2017)
	VARI	$VARI = \frac{Green - Red}{Green + Red - Blue}$	(Weiss et al., 1997)
	TGI	$TGI = Green - 0.39 \times Red - 0.61 \times Blue$	(Weiss et al., 1997)
	NDGI	$NDGI = \frac{Green - Red}{Green + Red}$	(Xue & Su, 2017)
	NGBDI	$NGDBI = \frac{Green - Blue}{Green + Blue}$	(Xue & Su, 2017)
	MGRVI	$MGRVI = \frac{Green^2 - Red^2}{Green^2 + Red^2}$	(Bendig et al., 2015)
	RGBVI	$RGBVI = \frac{Green^2 - Red \times Blue}{Green^2 + Red \times Blue}$	(Bendig et al., 2015)
	VEG	$VEG = \frac{Green}{Red^{0.667} \times Blue^{0.333}}$	(Hague et al., 2006)
	EXG	$EXG = 2 \times Green - Red - Blue$	(Woebbecke et al., 1995)

[1] Red: red band. NIR: near infrared band. NDVI: normalized diffrence vegetation index. RVI: ratio vegetation index. DVI: difference vegetation index. DRN: difference red-nir ratio. IPVI: infrared percentage vegetation index. VDVI: visible-band difference vegetation index. VARI: visible atmospheric resistant index. TGI: triangular greenness index. NDGI: normalized difference greenness index. NGBDI: normalized green blue difference index. MGRVI: modified green red vegetation index. RGBVI: red green blue vegetation index. VEG: vegetative index. EXG: excess of green index.

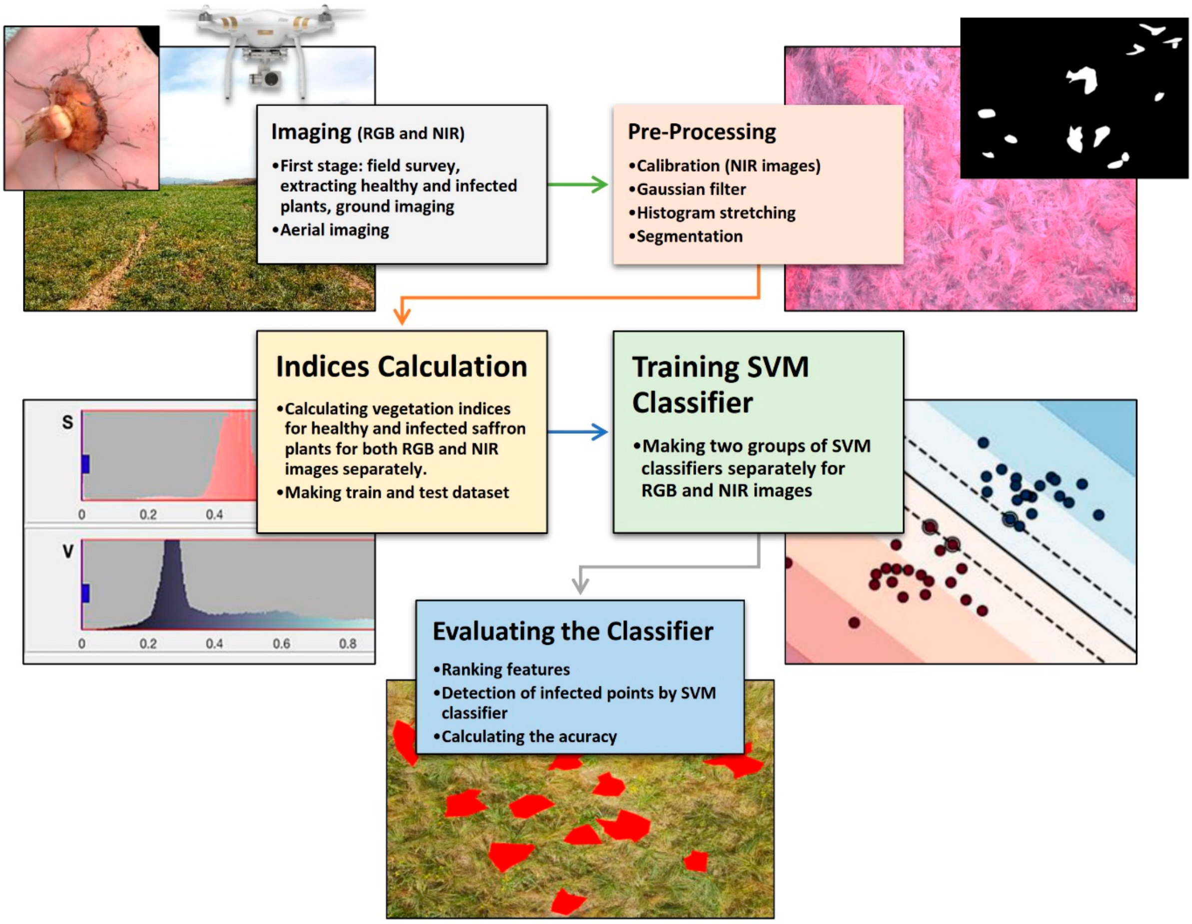

Figure 3. Workflow diagram of making a classifier model to detect the infested saffron plants by mite.

Prior to creating the dataset, NIR images required calibration, which was performed using "Mapir Camera Control" software (MAPIR, USA). The flowchart illustrating the dataset creation process is depicted in Figure 3. To separate infested and healthy saffron leaves, segmentation was performed on the images to create masks. This process was carried out individually for each image using MATLAB code or through manual cutting and separation of infested leaf sections. In some cases, where saffron plants exhibited minimal corm damage caused by mites, healthy and infested leaves were juxtaposed. For these instances, masking and separation were performed manually in Photoshop software, guided by information from field inspections and physically placed markers on the leaves.

Two datasets were generated for each image: the first containing a raw dataset of infested leaf pixels extracted from the main bands, and the second comprising a raw dataset of the main bands relating to healthy leaves. Both groups were utilized to calculate spectral indices (Table 3) for training the classifier.

Vegetation indices

In order to identify the required indices for a sound description of the infested areas and to maximise segmentation during the classification process, some indices were selected based on the available spectra extracted from the cameras (red, green, blue and 850nm NIR) according to the literature (Table 3). Since the infested and healthy plants were identical, the shape-based indices were discarded and the classification process was performed based on the spectral colour-based indices. As shown in Table 3, seven indices, including the Red, NIR, NDVI, RVI, difference vegetation index (DVI), difference red-nir ratio (DRN), and infrared percentage vegetation index (IPVI) were used to classify the infrared images. Besides, the reflectance in the main spectra of red, blue, green, and visible-band difference vegetation index (VDVI), visible atmospheric resistant index (VARI), triangular greenness index (TGI), normalized difference greenness index (NDGI), normalized green blue difference index (NGBDI), modified green red vegetation index (MGRVI), red green blue vegetation index (RGBVI), vegetative index (VEG), and excess of green index (EXG) were used to classify the RGB images.

Analysing and data modelling

The SVM, a supervised learning algorithm based on statistical learning theory, was adopted to detect and classify the infested plants from the healthy ones (Vani et al., 2017). Assuming class separability based on spectral index differences, hyperplanes with minimal margins were developed to distinguish between the classes. A dataset comprising randomly selected pixels and their corresponding indices from the total NIR images dataset for each group was created. These datasets included vegetation indices of 4000 pixels associated with healthy plants and 4000 pixels associated with infested ones. Ground survey data validated the accuracy of these groups. A similar procedure was followed for RGB images, resulting in two separate SVM structures: one for RGB images and one for NIR images. Eighty percent of the data was randomly selected for training, while the remaining 20% was used for validation (Baradaran Motie et al., 2021). The radial basis function (RBF) kernel was utilized in the SVM classifier. It is important to note that SVM models assign a class to each datum based on a decision-making function (Equation 1). Equation 2 presents the RBF kernel (Vani et al., 2017).

No significant differences were found between clusters in the composition, hygiene-sanitary parameters, and antioxidant capacity of the milk studied, as the animals in all farms were similarly managed based on the use of natural pastures. However, significant changes were observed in the milk composition by calendar month because of lactation effects and differences in feeding regimens. The percentage of lactose and the milk component yields (g d−1) patterns throughout the lactation months were similar, while the relationship between the fat and protein percentages was inverse to milk yield. During the end of summer and autumn months, the highest number of bacteria and somatic cells in the milk were observed, but the bacteriological count levels were below the legal limit set by EC regulations. The TAC was significantly higher in winter and spring milks than in the other milk samples.

The negative correlation between the antioxidant capacity and the somatic cells shows the important role of antioxidants in maintaining optimal udder health. One of the compounds involved in this antioxidant mechanism could be vitamin A due to the positive correlation between the antioxidant capacity and retinol determined in a previous study.

Finally, the information generated in this and previous studies on the quality of goat milk from the autochthonous Payoya breed will contribute to establishing the records of the traceability system to guarantee that the animal products obtained are of the native breed. All of this will help the consumer to easily identify these products and increase their demand, which will result in the conservation and promotion of the genetic heritage of these breeds and the foods derived from them.

$D(Z) = sign(\sum_{1}^{n} \alpha_i y_i K(Z.S_i) + b)$	(1)
$K(z.s) = e^{\frac{-\lvert z-s \rvert^2}{2\sigma^2}}$	(2)

In these equations, α is a constant coefficient, y is the group vector (labels), Si is the support vector, Z is the input vector, K (Z, Si) is the kernel of the SVM model, D(Z) is the decision function and σ is the variance.

To identify infested saffron plants, the generated SVM-based codes first processed the images, calculated vegetation indices, and applied the classification model. Furthermore, these developed SVM classifiers enabled the calculation of infestation proportions and the identification of corresponding areas within the field.

Software

To validate the SVM classifier models, two new datasets were created using images (NIR and RGB) from different fields acquired during the second year of imaging and not utilized in model development. These datasets comprised 30 aerial images, three RGB and three NIR, representing six images from each field.

The confusion matrix method was employed to evaluate classifier performance. To address the class imbalance resulting from a higher prevalence of healthy plants, an under-sampling technique was implemented. This involved

Table 4. Average, standard deviation, and t-test results for the image-based indices of healthy and infested saffron leaves for near-infrared images.

Index[1]	Healthy plant		Infested plant		t-test for equality of means p-value
	Average	SD[2]	Average	SD	
Red	131.6	31.5	153.1	20.0	0.000
NIR	236.6	21.1	221.8	24.6	0.007
NDVI	0.266	0.089	0.215	0.037	0.000
RVI	0.587	0.106	0.646	0.052	0.000
DVI	90.062	18.02	83.71	14.751	0.000
DRN	-0.755	0.430	-0.556	0.120	0.000
IPVI	0.633	0.045	0.608	0.045	0.006

[1] Red: red band. NIR: near infrared band. NDVI: normalized diffrence vegetation index. RVI: ratio vegetation index. DVI: difference vegetation index. DRN: difference red-nir ratio. IPVI: infrared percentage vegetation index. [2] Standard deviation.

Table 5. Average, standard deviation, and t-test results for the image-based indices of healthy and infested saffron leaves for RGB images.

Feature[1]	Healthy plant		Infested plant		t-test for equality of means p-value
	Average	SD[2]	Average	SD	
Red	117.7	45.2	147.3	38.2	0.000
Green	129.2	42.7	158.2	42.8	0.003
Blue	89.3	41.4	128.8	55.3	0.000
VDVI	0.134	0.105	0.079	0.067	0.000
VARI	0.089	0.111	0.064	0.091	0.048
TGI	28.77	12.52	22.16	15.80	0.067
NDGI	0.062	0.088	0.034	0.056	0.064
NGBDI	0.221	0.151	0.142	0.159	0.004
MGRVI	0.119	0.150	0.067	0.110	0.057
RGBVI	-0.360	0.092	-0.409	0.080	0.000
VEG	1.281	0.325	1.164	0.193	0.070
EXG	51.27	24.54	40.25	28.05	0.081

[1] VDVI: visible-band difference vegetation index. VARI: visible atmospheric resistant index. TGI: triangular greenness index. NDGI: normalized difference greenness index. NGBDI: normalized green blue difference index. MGRVI: modified green red vegetation index. RGBVI: red green blue vegetation index. VEG: vegetative index. EXG: excess of green index. [2] Standard deviation.

randomly sampling from the healthy class to maintain approximately equal class sizes. The developed model classified the images, generating a binary matrix indicating the positions of infected pixels. This matrix was termed "Model Prediction". Subsequently, a second matrix, referred to as "Actual," was manually created based on field survey data, containing the positions of pixels corresponding to infected plants at the same imaging points. By comparing the Actual and Model Prediction matrices, classification accuracy parameters were calculated. These parameters included 'true positive' (TP), 'true negative' (TN), 'false positive' (FP), and 'false negative' (FN), as presented in Table 6. Based on these data, classification quality criteria were calculated.

Classifier algorithm accuracy is represented as the ratio of correctly classified pixels to the total number of pixels. This is also known as Sensitivity (SNS) or True Positive Rate (TPR). The F1 score, or F Measure, reflects the balance between precision and TPR. In classification models, the ideal scenario is when both FP and FN approach zero. The F1 score ranges from zero to one, with higher values indicating better performance.

To develop a classification structure using SVM, model results were continually compared with actual data to optimize the model and minimize deviations from the original data. The SVM model aimed to reduce this deviation iteratively by identifying discrepancies from actual values and determining optimal hyperparameters for separating infested and healthy plants. Model optimization was conducted using the "fitsvm" function with 5-fold cross-validation. This process identified the optimal values for the hyperparameters gamma and C in the RBF kernel function, which correspond to the selection of values for box constraints and kernel scale. A larger C value results in a narrower boundary between the two datasets (infested and healthy groups). While higher classification quality can be achieved with larger C values, it increases the risk of misclassification during the testing phase due to potential errors in classifying borderline data.

The kernel scale parameter, inversely related to gamma, indicates the influence of each observation on the model's

Table 6. Calculated parameters of the confusion matrix for the detection of infested saffron plants in RGB and NIR images in validation phase. The numbers are in pixel unit. Positive (class 1): infested, Negative (class 0): healthy.

Imaging mode	Total	TP	TN	FP (Type I error)	FN (Type II error)	Accuracy	Sensitivity	Specificity	Precision	F1
NIR	500	177	201	45	77	0.756	0.697	0.817	0.797	0.744
RGB	2004	773	837	165	229	0.803	0.771	0.835	0.824	0.797

NIR: Near infra red. RGB: red, green, blue. TP: True Positive, TN: True Negative, FP: False Positive, FN: False Negative, F1: The F1-score of a classifier.

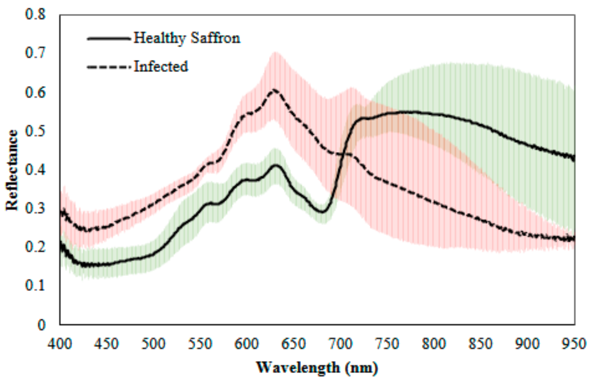

Figure 4. The spectral reflectance of healthy and mite infested saffron leaves recorded with the HYPSIM desktop hyperspectral camera. The black lines show the average reflectance at each wavelength and the shadows show the reflectance variations of the different samples at each wavelength.

output during training. Smaller kernel scale values are preferable as they suggest greater model stability. Additionally, the receiver operating characteristic (ROC) curve was employed as another evaluation metric to assess model performance. The ROC curve represents the area under the curve (AUC), and a value close to 1 indicates superior model performance.

Results

Five fields were selected based on reported infestations of the saffron bulb mite. Mite damage leads to saffron corm rot, characterized by plant withering, leaf yellowing and wilting, and a tawny to black, decayed, and soft appearance of infested corms (Figure 1). Mite pest prevalence in these fields was substantial, with an average of three out of ten plants exhibiting bulb mite damage when removed from the soil. Damaged corms exhibited over 70% rot.

Figure 4 illustrates the average spectral reflectance of leaves from healthy and mite-infested saffron plants within the Vis-NIR spectrum. A clear distinction exists between the spectral reflectance of healthy and infected plant leaves in both the visible (600-650 nm) and near-infrared (800-850 nm) spectra. Infected plants demonstrated higher reflectance in the visible region and lower reflectance in the NIR region, likely due to a decrease in chlorophyll content compared to healthy plants(Knipling, 1970). These results validate the wavelengths utilized by the cameras for identifying infested plants.

Vegetation indices

To initiate the analytical process, preliminary correlation coefficients between all indices (features) and descriptive

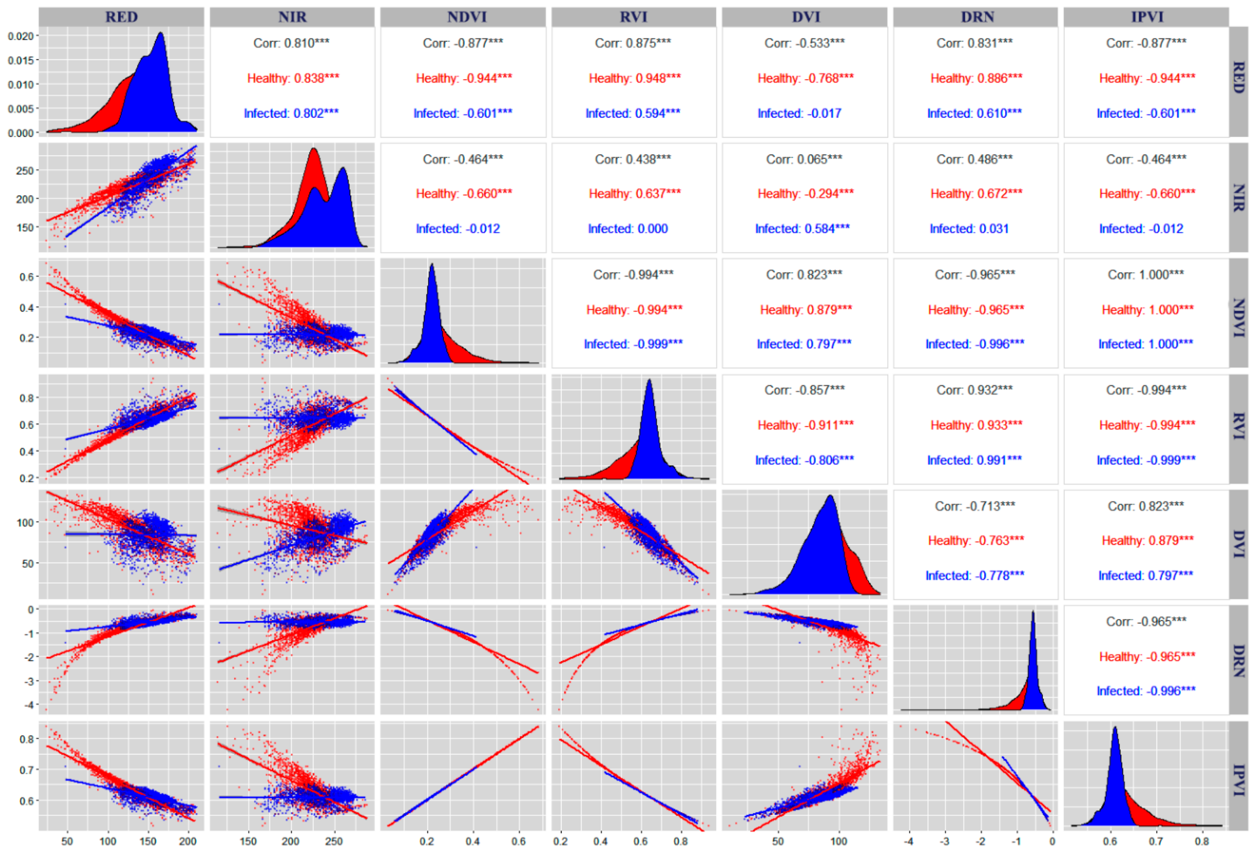

Figure 5. Pearson correlation matrix between the indices for NIR images of healthy and mite infested saffron plants. The numbers within the boxes indicate the correlation coefficients (black: all data, blue: infested, and red: healthy) and the significance levels of difference (*** significant at 0.01 level) between groups of data. The lower side of the matrix presents the scatter plot of indices in pairs in two healthy and infested groups.

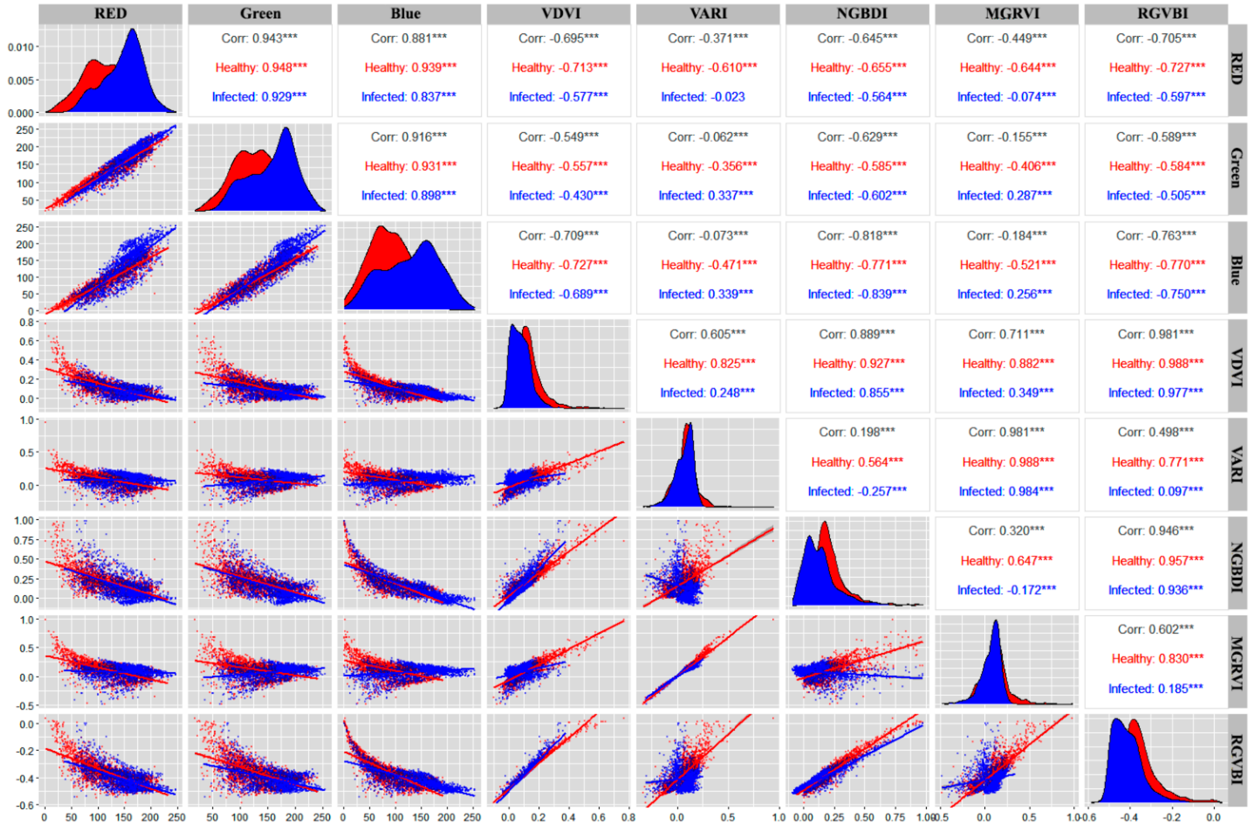

Figure 6. Pearson correlation matrix between the input variables for RGB images of healthy and mite infested saffron plants. The numbers within the boxes indicate the correlation coefficients (black: all data, blue: infested, and red: healthy) and significance levels (*** significant at 0.01 level) between the independent variables. The lower side of the matrix presents the scatter plot of features in pairs in two healthy and infested groups.

statistics were calculated. A dataset was prepared, encompassing images with selective masks for healthy and infested plants, including all five fields across two years of imaging. Table 4 presents the mean, standard deviation, and t-test results for the calculated indices (Table 3) of healthy and infested plants in NIR images. The results revealed that damaged plants exhibited higher average reflectance in the red band compared to healthy plants, while conversely, NIR band reflectance values were lower. The NDVI index, indicative of plant greenness, was on average 23.7% lower in damaged plants than in healthy plants (Devadas et al., 2009). Significant differences ($p < 0.01$) were observed between the values of the two groups (healthy and infested) for all indices. However, the standard deviation analysis indicated a wide dispersion of data, resulting in overlapping values between the two groups, as visualized in Figure 5. This suggests that no single index could effectively differentiate between healthy and infested saffron plants.

Figure 5 summarizes the pearson correlation coefficient (PCC) between indices and presents scatter plots depicting index changes relative to each other within the two groups (healthy and infested). These plots revealed distinct trends between the indices of the two groups, particularly for NIR-NDVI, NIR-RVI, NIR-DVI, NIR-DRN, and NIR-IPVI, suggesting potential for differentiating and classifying the groups. To distinguish between healthy and infested saffron plants, identifying distinct trends in the cross-changes of indices between the two groups is crucial. For instance, the NIR-NDVI plot (Figure 5) demonstrates a lack of correlation between the NIR index and NDVI of the infested group (correlation coefficient -0.012), whereas a correlation coefficient of -0.66 is observed for the healthy group. This highlights the importance of including both indices in the classification model. Conversely, in the cross-correlation plot of certain indices, such as RVI-NDVI, a high correlation coefficient between the values of the two groups (0.994 for healthy and 0.999 for infested) is evident. However, the pattern of change remains similar, with significant overlap between the data (scatter plot - Figure 5). Similar observations can be made for DRN-NDVI, DRN-RVI, IPVI-RVI, IPVI-NDVI, and IPVI-DRN.

Likewise, for RGB images, the descriptive statistics as well as the results of the t-test for healthy and infested plants are presented in Table 5. It reveals that, while there was no statistically significant difference between the mean values of infested and healthy plants in MGRVI, EXG, and VEG indices, the mean value of EXG in healthy plants was approximately 25% higher than in infested plants. However, the standard deviation indicates some overlap between the two groups, suggesting that this index may not be sufficient for individual group differentiation.

The PCC matrix and the scatter plot of the features which selected in the feature selection process relative

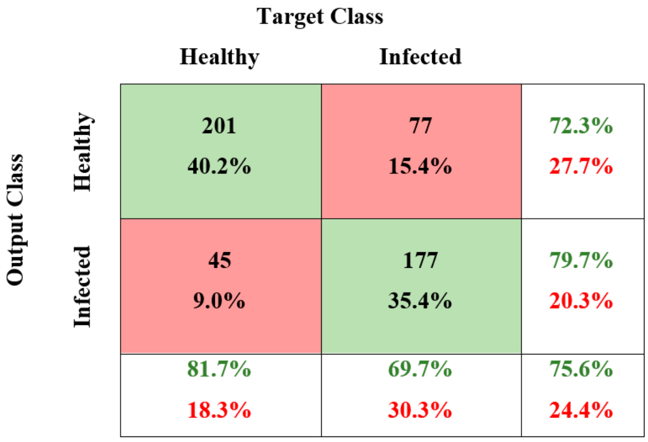

Figure 7. Confusion matrix for classifying infested saffron plants by mites in NIR images. Overall 75.6% of the data has been well categorized.

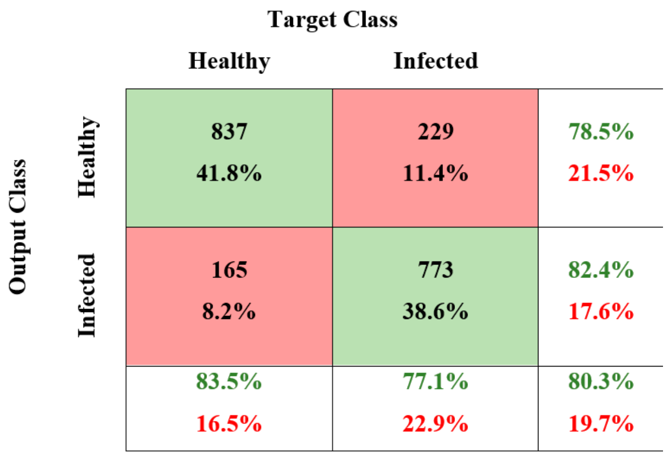

Figure 8. Confusion matrix for classifying infested saffron plants by mites in RGB images. Overall 80.3% of the data has been well categorized.

to healthy and infested groups are presented in Figure 6. The feature selection process identified Red, Green, Blue, VDVI, VARI, NGBDI, MGRVI, and RGVBI as essential features for the classification model, a finding supported by t-test results ($p < 0.01$) (Table 5). The average values of the primary RGB bands ((red+green+blue)/3) were higher in infested plants compared to healthy plants, indicating a brighter color in infected leaves.

Evaluation and validation of the SVM models

The training and testing steps for evaluating the best objective function after 30 iterations of NIR images revealed optimal C (Box-Constraint) and kernel scale values of 386.4 and 34.41, respectively. The model's accuracy in the testing phase reached 82.3%. Similarly, the SVM classifier with the radial basis function was used to classify RGB images. The training and testing steps for evaluating the best objective function identified optimal C (Box-Constraint) and kernel scale values of 205.6 and 74.23, respectively. The resulting classifier model achieved a testing stage accuracy of 91.4%.

The performance of the classifier models is presented in two confusion matrices, with their parameters summarized in Table 6 for both RGB and NIR models. The confusion matrices shown in Figures 7 and 8 demonstrate that over 75.6% and 80.3% of the data were correctly categorized for NIR and RGB images, respectively.

The RGB-SVM model exhibited a marginally higher AUC compared to the NIR-SVM model, as evidenced by the ROC curves (Figure 9). Therefore, based on the obtained results and the ease of using an RGB camera, the RGB-SVM detection system is recommended.

The developed SVM models could discriminate mite infested plants with an acceptable level of performance and accuracy. Low FN (false negative) values (Table 6)

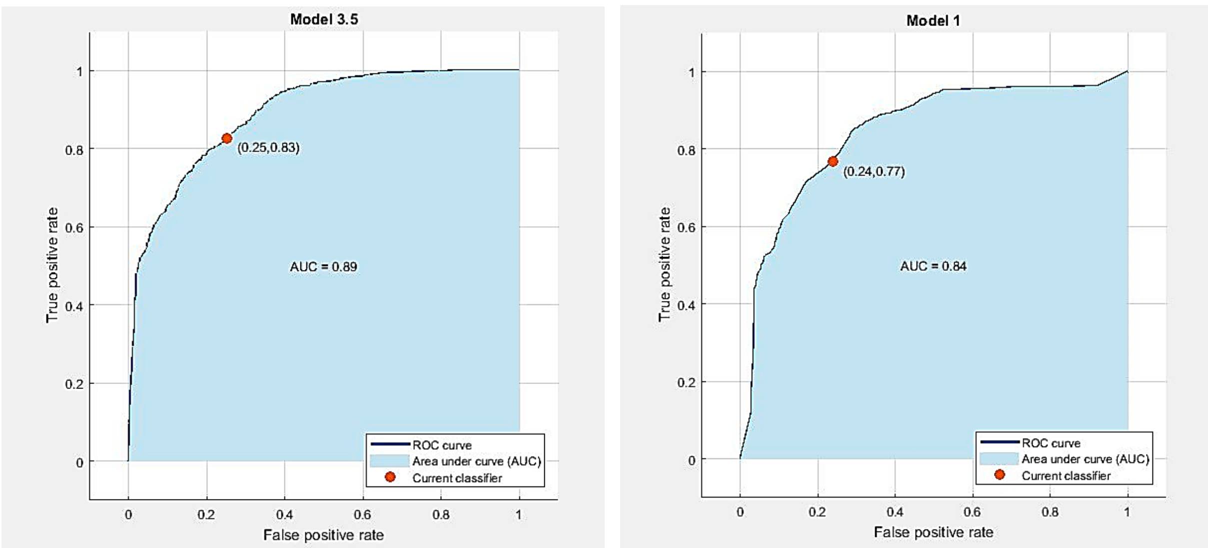

Figure 9. ROC curve and AUC of the SVM classifier models for detection of mite infested saffron plants. Left: RGB images classifier, Right: NIR images classifier.

suggest that there is little chance of missing the infested plants. However, the results for FP (false positive) show that, because of the small variation in their spectral reflectance, healthy plants could be identified as infested ones. Additionally, the F1 and sensitivity values are close to 0.7, indicating that the SVM classifier is performing as expected. To sum up the findings, the analysis shows that the classification model generates results that are both highly accurate and broadly applicable. The MATLAB code, running on a Core i7 CPU with 4 gigabytes of RAM, processed each aerial image in less than 15 seconds.

Discussion

This study investigated the feasibility of distinguishing mite-infested saffron plants from healthy plants using aerial imaging, image processing, and machine learning techniques. Five saffron fields were imaged in two consecutive years during the vegetative stage (when plants have leaves) in both RGB and near-infrared bands. After processing, the images were classified using the SVM classifier models and the efficiency of the models were verified.

The analysis of the Red band reflectance (660 nm wavelength) showed that the reflectance of the infested plant's leaves was significantly higher than those of the healthy ones. This was due to some colour changes on the leaf tips, indicating the effects of fungal damage (caused by mites) on the plant, leading to weakness and reduced chlorophyll-a, which absorbs red band. The average of NIR (850 nm) values of the damaged plants were significantly lower than those of the healthy plants (the diagonal diagrams of Figure 5). These results are consistent with those reported by Genc et al. (2008) and di Gennaro et al. (2016). The NDVI index, widely used in vegetation monitoring (Weiss et al., 1997), demonstrated higher values in healthy plants due to their significantly higher near-infrared reflectance compared to infested plants (Govaerts & Verhulst, 2010). The average of NDVI values of the damaged plants (0.215) were significantly lower than those of the healthy plants (0.266). The mean of the RVI index of damaged plants was higher than those of the healthy ones, as they had a considerably higher reflectance in the RED band and lower reflectance in the NIR band, raising the RVI index. However, healthy plants had higher DVI values than unhealthy plants because they absorb more significant amounts of Red band wavelength than infested plants, this is consistent with Silva et al. (2004) findings. Moreover, the mean value of the DRN index was much smaller in healthy plants than in infested plants. Therefore, this index was able to distinguish infested plants from healthy ones. The IPVI index displayed minimal variation between damaged and healthy plants across all studied fields.

Analysis of RGB image indices revealed that VDVI values in damaged plants varied within a narrow range. This variation can be attributed to mite and fungal damage, resulting in decreased photosynthetic activity. Higher VDVI values generally indicate healthier and denser vegetation (Du & Noguchi, 2017). However, in this study, the VARI index proved insufficient for individually distinguishing between damaged and healthy plants. No statistically significant difference was observed in the VARI mean value between the two groups. The TGI index values for infested plants were lower than those of healthy plants, as shown in Table 5 and Figure 6. A higher TGI value generally signifies a healthier plant with a higher chlorophyll-a content. While no statistically significant difference was found between the TGI values of healthy and infested plants, the NDGI index results align with those reported by Phadikar, et al., (2013), according to which the mean NDGI value for the healthy saffron plants was higher than that of the infested plants. The NGBDI describe the vegetation using reflectance in Green and Blue spectra (Du & Noguchi, 2017), higher value of the NGBDI suggests healthier status of the intended plants (Brenner et al., 2018). As found in this study, the average of the NGBDI for infested plants was significantly lower than that of the healthy plants.

This study demonstrated the capability of Vis-NIR aerial imaging to differentiate between similar infested and healthy saffron plants. The analysis of proposed indices for NIR and RGB images revealed a narrow boundary separating the characteristics of healthy and infested saffron plants, with a considerable portion of the two groups overlapping within this boundary (Figures 5 and 6). To achieve acceptable discrimination accuracy, multiple spectral indices were simultaneously employed in the developed SVM models (Rumpf et al., 2010; Carreño-Conde et al., 2021).

The average accuracy of the detection system was 91.4% and 82.3% respectively for using SVM models based on RGB images and NIR images. The results are in line with those reported for other plant disease detection models based on processing leaves symptoms. For example, 88.1% accuracy for powdery mildew detection in wheat plant (Hussein & Abbas, 2019), 92.6% for early blight detection on potato leaves (Abdu et al., 2020) and 95% accuracy for rice paddy disease detection (Chawal & Panday, 2019) using different types of SVM classifiers. This study focused on using aerial images captured by a drone, incorporating index selection for potential commercial in-line application, which may be more suitable for precision spraying than manual in-field classification. In scenarios requiring on-the-go image analysis, reducing the number of indices to three could potentially accelerate model processing time. The combination of aerial imaging, machine learning models, and SVM classifiers offers a practical solution for detecting infestations in saffron fields.

Conclusion

This study investigated the possibility of identifying infested saffron plants with their corms damaged by mites and fungi using RGB and NIR images. Mites infest saffron corms, and the resulting damage often remains concealed underground. The effects of this damage become apparent in the outer plant parts at a later stage, making visual detection challenging, even for experts. The fungal infestation of saffron plants, often caused by mites, is a complex process. As a result, the ability to detect contamination in the field can still help saffron producers, even if not very accurately. Aerial imaging, with its acceptable performance, rapid surveying speed, and timely results, presents a viable solution. The SVM model, employing the RBF kernel, offers a robust method for distinguishing infested saffron plants from healthy ones.

Data availability: Data will be available on request

Competing interests: The authors have declared that no competing interests exist.

Authors' contributions: Hossein Sahabi: Conceptualization, Formal analysis, Funding acquisition, Investigation, Project administration, Supervision, Writing – review & editing. Jalal Baradaran-Motie: Conceptualization, Data curation, Formal analysis, Investigation, Methodology, Visualization, Writing – original draft, Writing – review & editing.

Funding agencies/ institutions:	Project / Grant
Saffron Institute, University of Torbat Heydarieh, Iran	P/100252

References

Abbas A, Jain S, Gour M, Vankudothu S, 2021.Tomato plant disease detection using transfer learning with C-GAN synthetic images. Comput. Electron. Agric. 187:106279. https://doi.org/10.1016/j.compag.2021.106279

Abdelghafour F, Sivarajan SR, Abdelmeguid I, Ryckewaert M, Roger JM, Bendoula R, Alexandersson E, 2023.Including measurement effects and temporal variations in VIS-NIRS models to improve early detection of plant disease: Application to Alternaria solani in potatoes. Comput. Electron. Agric. 211:107947. https://doi.org/10.1016/j.compag.2023.107947

Abdu AM, Mokji MMM, Sheikh UUU, 2020. Machine learning for plant disease detection: an investigative comparison between support vector machine and deep learning. IAES Int. J. Artif. Intell. 9:670. https://doi.org/10.11591/ijai.v9.i4.pp670-683

Abdulridha J, Ampatzidis Y, Roberts P, Kakarla SC, 2020. Detecting powdery mildew disease in squash at different stages using UAV-based hyperspectral imaging and artificial intelligence. Biosyst. Eng. 197:135-148. https://doi.org/10.1016/j.biosystemseng.2020.07.001

Abuleil AM, Taylor GW, Moussa M, 2015. An Integrated System for Mapping Red Clover Ground Cover Using Unmanned Aerial Vehicles: A Case Study in Precision Agriculture. In: Proceedings -2015 12th Conference on Computer and Robot Vision, CRV 2015. IEEE pp. 277-284. https://doi.org/10.1109/CRV.2015.43

Armstrong P, Maghirang E, Ozulu M, 2019. Determining damage levels in wheat caused by Sunn pest, Eurygaster integriceps) using visible and near-infrared spectroscopy. J. Cereal Sci. 86:102-107. https://doi.org/10.1016/j.jcs.2019.02.003

Aslahishahri M, Stanley KG, Duddu H, Shirtliffe S, Vail S, Bett K, Pozniak C, Stavness I, 2021. From RGB to NIR: Predicting of near infrared reflectance from visible spectrum aerial images of crops. In: 2021 IEEE/CVF International Conference on Computer Vision Workshops, ICCVW).Vol. 2021- Octob IEEE pp. 1312-1322. https://doi.org/10.1109/ICCVW54120.2021.00152

Ballesteros R, Ortega JF, Hernández D, Moreno MA, 2014. Applications of georeferenced high-resolution images obtained with unmanned aerial vehicles. Part I: Description of image acquisition and processing. Precis. Agric. 15:579-592. https://doi.org/10.1007/s11119-014-9355-8

Baradaran Motie J, Aghkhani MH, Rohani A, Lakzian A, 2021. A soft-computing approach to estimate soil electrical conductivity. Biosyst. Eng. 205:105-120. https://doi.org/10.1016/j.biosystemseng.2021.02.015

Baradaran Motie J, Saeidirad MH, Jafarian M, 2023. Identification of Sunn-pestaffected, Eurygaster Integriceps put.) wheat plants and their distribution in wheat fields using aerial imaging. Ecol. Inform. 102146. https://doi.org/10.1016/j.ecoinf.2023.102146

Basati Z, Jamshidi B, Rasekh M, Abbaspour-Gilandeh Y, 2018. Detection of sunn pest-damaged wheat samples using visible/near-infrared spectroscopy based on pattern recognition. Spectrochim. Acta Part A Mol. Biomol. Spectrosc. 203:308-314. https://doi.org/10.1016/j.saa.2018.05.123

Bendig J, Yu K, Aasen H, Bolten A, Bennertz S, Broscheit J, Gnyp ML, Bareth G, 2015.Combining UAV-based plant height from crop surface models, visible, and near infrared vegetation indices for biomass monitoring in barley. Int. J. Appl. Earth Obs. Geoinf. 39:79-87. https://doi.org/10.1016/j.jag.2015.02.012

Brenner C, Zeeman M, Bernhardt M, Schulz K, 2018. Estimation of evapotranspiration of temperate grassland based on high-resolution thermal and visible range imagery from unmanned aerial systems. Int. J. Remote Sens. 39:5141-5174. https://doi.org/10.1080/01431161.2018.1471550

Caiola MG, Canini A, 2010. Looking for saffron's, Crocus sativus L.) parents. Funct. Plant Sci. Biotechnol. 4:1-14

Camargo A, Smith JS, 2009. An image-processing based algorithm to automatically identify plant disease visual symptoms. Biosyst. Eng. 102:9-21. https://doi.org/10.1016/j.biosystemseng.2008.09.030

Cardone L, Castronuovo D, Perniola M, Cicco N, Candido V, 2020. Saffron, Crocus sativus L.), the king of spices: An overview. Sci. Hortic., Amsterdam). 272:109560. https://doi.org/10.1016/j.scienta.2020.109560

Carreño-Conde F, Sipols AE, Simón C, Mostaza-Colado D, 2021. A forecast model applied to monitor crops dynamics using vegetation indices, Ndvi). Appl. Sci. 11:1-25. https://doi.org/10.3390/app11041859

Cerqueira DTR de, Raetano CG, Pogetto MHF do AD, Carvalho MM, Prado EP, Costa SÍ de A, Moreira CAF, 2017. Optimization of spray deposition and Tetranychus urticae control with air assisted and electrostatic sprayer. Sci. Agric. 74:32-40. https://doi.org/10.1590/1678-992x-2015-0340

Chawal B, Panday SP, 2019. Rice Plant Disease Detection using Twin Support Vector Machine, TSVM). J. Sci. Eng. 7:61-69. https://doi.org/10.3126/jsce.v7i0.26794

Crippen RE, 1990.Calculating the vegetation index faster. Remote Sens. Environ. 34:71-73. https://doi.org/10.1016/0034-4257(90)90085-Z

Devadas R, Lamb DW, Simpfendorfer S, Backhouse D, 2009. Evaluating ten spectral vegetation indices for identifying rust infection in individual wheat leaves. Precis. Agric. 10:459-470. https://doi.org/10.1007/s11119-008-9100-2

Du M, Noguchi N, 2017. Monitoring of Wheat Growth Status and Mapping of Wheat Yield's within-Field Spatial Variations Using Color Images Acquired from UAV-camera System. Remote Sens. 9:289. https://doi.org/10.3390/rs9030289

Elarab M, Ticlavilca AM, Torres-Rua AF, Maslova I, McKee M, 2015. Estimating chlorophyll with thermal and broadband multispectral high resolution imagery from an unmanned aerial system using relevance vector machines for precision agriculture. Int. J. Appl. Earth Obs. Geoinf. 43:32-42. https://doi.org/10.1016/j.jag.2015.03.017

di Gennaro SF, Battiston E, di Marco S, Facini O, Matese A, Nocentini M, Palliotti A, Mugnai L, 2016 .Unmanned Aerial Vehicle, UAV)-based remote sensing to monitor grapevine leaf stripe disease within a vineyard affected by esca complex. Phytopathol. Mediterr. 55:262-275.

Golmohammadi F, 2014. Saffron and its farming, economic importance, export, medicinal characteristics and various uses in South Khorasan Province-East of Iran. Int. J. Farming Allied Sci. 3:566-596

Gómez-Casero MT, Castillejo-González IL, García-Ferrer A, Peña-Barragán JM, Jurado-Expósito M, García-Torres L, López-Granados F, 2010. Spectral discrimination of wild oat and canary grass in wheat fields for less herbicide application. Agron. Sustain. Dev. 30:689-699. https://doi.org/10.1051/agro/2009052

Gomez C, Viscarra Rossel RA, McBratney AB, 2008. Soil organic carbon prediction by hyperspectral remote sensing and field vis-NIR spectroscopy: An Australian case study. Geoderma 146:403-411. https://doi.org/10.1016/j.geoderma.2008.06.011

Govaerts B, Verhulst N, 2010. The Normalized Difference Vegetation Index, NDVI) GreenSeeker TM Handheld Sensor: Toward Integrated Evaluation of Crop Management. Part B: User Guide. Cimmyt 12.

Gulhane M, Gurjar A, 2011. Detection of diseases on cotton leaves and its possible diagnosis. Int. J. Image Process. 5:590-598

Hague T, Tillett ND, Wheeler H, 2006.Automated Crop and Weed Monitoring in Widely Spaced Cereals. Precis. Agric. 7:21-32. https://doi.org/10.1007/s11119-005-6787-1

Hussein M, Abbas AH, 2019. Plant Leaf Disease Detection Using Support Vector Machine. Al-Mustansiriyah J. Sci. 30:105-110. https://doi.org/10.23851/mjs.v30i1.487

Jin X, Shi C, Yu CY, Yamada T, Sacks EJ, 2017. Determination of leaf water content by visible and near-infrared spectrometry and multivariate calibration in Miscanthus. Front. Plant Sci. 8:721. https://doi.org/10.3389/fpls.2017.00721

Kafi M, Koocheki A, Rashed MH, Nassiri M, 2006. Saffron, Crocus sativus) production and processing. Science Publishers. https://doi.org/10.1201/9781482280463

Knipling EB, 1970. Physical and physiological basis for the reflectance of visible and near-infrared radiation from vegetation. Remote Sens. Environ. 1:155-159. https://doi.org/10.1016/S0034-4257(70)80021-9

Li W, Wang D, Li M, Gao Y, Wu J, Yang X, 2021. Field detection of tiny pests from sticky trap images using deep learning in agricultural greenhouse. Comput. Electron. Agric. 183:106048. https://doi.org/10.1016/j.compag.2021.106048

Mohamed ES, Saleh AM, Belal AB, Gad AA, 2018. Application of near-infrared reflectance for quantitative assessment of soil properties. Egypt. J. Remote Sens. Sp. Sci. 21:1-14. https://doi.org/10.1016/j.ejrs.2017.02.001

Mzabri, Addi, Berrichi, 2019.Traditional and Modern Uses of Saffron, Crocus Sativus). Cosmetics 6:63. https://doi.org/10.3390/cosmetics6040063

Phadikar S, Sil J, Das AK, 2013. Vegetative indices and edge texture based shadow elimination method for rice plant images. In: 2012 International Conference on Radar, Communication and Computing, ICRCC). IEEE pp. 1-5. https://doi.org/10.1109/ICRCC.2012.6522596

Rahimi H, Nateq Golestan M, Kakhki A, 2018. Exploring the impact of non-chemical methods on the control of bulb mite, Rhizoglyphus robini Claparáde) and yield of saffron, Crocus sativus L.). New Zeal. Plant Prot. 71:93-101. https://doi.org/10.30843/nzpp.2018.71.108

Rumpf T, Mahlein AK, Steiner U, Oerke EC, Dehne HW, Plümer L, 2010. Early detection and classification of plant diseases with Support Vector Machines based on hyperspectral reflectance. Comput. Electron. Agric. 74:91-99. https://doi.org/10.1016/j.compag.2010.06.009

Rupesh G. Mundada RGM, 2013. Detection and Classification of Pests in Greenhouse Using Image Processing. IOSR J. Electron. Commun. Eng. 5:57-63. https://doi.org/10.9790/2834-565763

Sankaran S, Khot LR, Espinoza CZ, Jarolmasjed S, Sathuvalli VR, Vandemark GJ, Miklas PN, Carter AH, Pumphrey MO, Knowles RRN, Pavek MJ, 2015. Low-altitude, high-resolution aerial imaging systems for row and field crop phenotyping: A review. Eur. J. Agron. 70:112-123. https://doi.org/10.1016/j.eja.2015.07.004

Silleos NG, Alexandridis TK, Gitas IZ, Perakis K, 2006. Vegetation Indices: Advances Made in Biomass Estimation and Vegetation Monitoring in the Last 30 Years. Geocarto Int. 21:21-28. https://doi.org/10.1080/10106040608542399

Silva JMN, Cadima JFCL, Pereira JMC, Grégoire JM, 2004. Assessing the feasibility of a global model for multi-temporal burned area mapping using SPOT-VEGETATION data. Int. J. Remote Sens. 25:4889-4913. https://doi.org/10.1080/01431160412331291251

Tavakkoli-Korghond G, Sahebzadeh N, 2022. A modified method for mass production of generalist predatory edaphic mite Gaeolaelaps aculeifer as a candidate for biological control of the saffron corm mite. https://doi.org/10.1080/01647954.2022.2043936 48:159-164. https://doi.org/10.1080/01647954.2022.2043936

Vani N, Sowmya A, Jayamma N, 2017. Brain Tumor Classification using Support Vector Machine. Int. Res. J. Eng. Technol. 4:792-796.

Wang X, Wang M, Wang S, Wu Y, 2015. Extraction of vegetation information from visible unmanned aerial vehicle images. Nongye Gongcheng Xuebao/Transactions Chinese Soc. Agric. Eng. 31:152-159

Warren G, Metternicht G, 2005. Agricultural applications of high-resolution digital multispectral imagery: Evaluating within-field spatial variability of canola, Brassica napus) in Western Australia.

Photogramm. Eng. Remote Sensing 71:595-602. https://doi.org/10.14358/PERS.71.5.595

Weiss MJ, Hofeldt AJ, Behrens M, Fisher K, 1997. Ocular siderosis: Diagnosis and management. Retina 17:105-108. https://doi.org/10.1097/00006982-199703000-00004

Woebbecke DM, Meyer GE, Von Bargen K, Mortensen DA, 1995. Color Indices for Weed Identification Under Various Soil, Residue, and Lighting Conditions. Trans. ASAE 38:259-269. https://doi.org/10.13031/2013.27838

Xiang H, Tian L, 2011. Development of a low-cost agricultural remote sensing system based on an autonomous unmanned aerial vehicle, UAV). Biosyst. Eng. 108:174-190. https://doi.org/10.1016/j.biosystemseng.2010.11.010

Xue J, Su B, 2017. Significant Remote Sensing Vegetation Indices: A Review of Developments and Applications. J. Sensors 2017:1-17. https://doi.org/10.1155/2017/1353691

Yang CM, Cheng CH, Chen RK, 2007 .Changes in spectral characteristics of rice canopy infested with brown planthopper and leaffolder. Crop Sci. 47:329-335. https://doi.org/10.2135/cropsci2006.05.0335

Zakiaghl M, Khorramdel S, Koocheki A, Nabati J, Nezami A, Mirshamsi Kachki A, Mollafilabi A, Rezvani Moghaddam P, Nassiri Mahallati M, 2021. Criteria for production of standard pathogen-free saffron corms. Saffron Agron. Technol. 9:121-141

Zarco-Tejada PJ, Guillén-Climent ML, Hernández-Clemente R, Catalina A, González MR, Martín P, 2013. Estimating leaf carotenoid content in vineyards using high resolution hyperspectral imagery acquired from an unmanned aerial vehicle, UAV). Agric. For. Meteorol. 171-172:281-294. https://doi.org/10.1016/j.agrformet.2012.12.013